

A mean-field approach to the propagation of field patterns in stratified magneto rotational turbulence

Oliver Gressel*

Astronomy Unit, Queen Mary, University of London, Mile End Road, London E1 4NS, United Kingdom

Accepted 1988 December 15. Received 1988 December 14; in original form 1988 October 11

ABSTRACT

Local shearing box simulations of stratified magneto rotational turbulence invariably exhibit cyclic field patterns which propagate away from the disc midplane. A common explanation for this is magnetic buoyancy. The recent analysis by Shi et al. however shows that the flow is buoyantly stable below one disc scale height H , necessitating an alternative explanation in this region.

We here conduct and analyse direct numerical simulations to explain the observed behaviour by means of a mean-field description. Apart from the mean radial and azimuthal field, we monitor the small-scale current helicity, which we propose as a key indicator for saturation.

Reconstructing the horizontally averaged field, we demonstrate that the problem can be reduced to a one-dimensional induction equation. By means of the so-called test field method, we then determine the underlying closure parameters. Our analysis shows that, apart from a possible *direct* MRI dynamo, two distinct *indirect* dynamo mechanisms operate in the disc. This resolves the issue of the “wrong” sign of the MRI dynamo effect.

Finally, we use the obtained closure parameters to run a dynamically quenched dynamo model. This model approximately recovers the observed field patterns in the mean fields. Moreover, the model reproduces the prevailing parity and the distinct phase pattern in the small-scale current helicity. The latter property might open a potential route to understand the saturation of MRI induced turbulence.

Key words: accretion discs – magnetohydrodynamics (MHD) – methods: numerical

1 INTRODUCTION

Recent numerical findings have challenged the sustainability of hydromagnetic turbulence driven by the magneto rotational instability (MRI, Balbus & Hawley 1998), and hence the viability of the approach to provide the turbulent viscosity needed to explain accretion luminosities (King et al. 2007).

The fundamental mechanism of the MRI relies on the interplay between the epicyclic and magnetic restoring forces. A *coherent* magnetic field acts as the mediator to extract free energy from the Keplerian rotation. Unless maintained by an external source or a helical dynamo, such a coherent field is, however, prone to dissipation by the turbulence created via parasitic instabilities (Goodman & Xu 1994; Pessah & Goodman 2009; Latter et al. 2009). This becomes apparent when looking at the most simplified case:

Pessah et al. (2007) have analysed the results of a set of unstratified local MRI simulations. The scaling law they derive predicts turbulent stresses based on several input parameters. For

the case without vertical net-flux, they conclude that simulation results should depend linearly on the numerical resolution. Fromang & Papaloizou (2007) have independently confirmed this prediction and show that transport coefficients do not converge with increasing resolution. This finding of vanishing turbulent stresses W_{xy} for zero net flux (ZNF) is in contrast to the case of a net vertical flux (NVF), which continuously drives long-wavelength MRI modes (see discussion in Pessah et al. 2007), and for which convergence has been obtained (Davis et al. 2009).

Fromang & Papaloizou (2007) attribute the lack of convergence to a resolution-dependent effective Prandtl number Pm_{num} of their code. In a subsequent paper, Fromang et al. (2007) show that convergence can be recaptured if explicit dissipation with $Pm \gtrsim 2$ is included. For smaller values of Pm , the lack of convergence may be attributed to the fact that a small-scale dynamo becomes much harder to excite (Schekochihin et al. 2005). An alternative interpretation has been put forward by Kitchatinov & Rüdiger (2009), who relate the convergence issue to the problem of resolving radial structures occurring for non-axis symmetric MRI modes.

But how realistic are such local models? Vishniac (2009) has recently pointed out that unstratified local simulations do not pro-

* E-mail: o.gressel@qmul.ac.uk

vide a (physically relevant) outer scale for the turbulence, and therefore the observed Pm dependence might be an artifact of the local approximation.

Davis et al. (2009) indeed report characteristic differences in magnetic power spectra for VNF and ZNF simulations, illustrating the lack of a well-defined injection scale in the latter case. Since the eddy viscosity is determined by the outer scale, this is sufficient to explain the convergence in W_{xy} for ideal MHD. Note that Lesur & Longaretti (2007), however, found a strong trend towards weaker turbulence for smaller explicit Pm in unstratified NVF simulations.

Regardless of the Pm dependence, coherent field structures appear to be the prerequisite for driving significant accretion stresses. Moreover, large-scale fields may even contribute to the accretion stresses directly (see e.g. Fig. 8 in Johansen & Levin 2008). In the absence of external fields, a mean-field dynamo can provide a means to replenish coherent fields that in turn drive MRI. This idea has first been advocated by Brandenburg et al. (1995). Such an effect is likely beneficial to sustain MRI turbulence, possibly even at $Pm \ll 1$ as the excitation conditions of large-scale dynamos are known to be independent of Pm (Brandenburg 2009). In fact, Davis et al. (2009) have very recently shown that stratification provides a sufficient condition for convergence in the ZNF case and attribute this to a dynamo-generated mean azimuthal field (also cf. Shi et al. 2009). If this is the case, the saturation amplitude of W_{xy} should depend on the quenched state of the underlying dynamo.

Along these lines, it becomes mandatory to better understand how accretion discs can maintain coherent fields – overcoming both turbulent dissipation and buoyant field expulsion. As advocated in Blackman (2010), understanding the non-linear saturation of MRI in a realistic scenario will require to couple a closure model for turbulent stresses with mean-field dynamo theory. As for the former, approaches beyond a simple Shakura-Sunyaev viscosity include phenomenological closures by Ogilvie (2003) (ZNF), Pessah et al. (2006a) (VNF), and Hubbard & Blackman (2008). The applicability of these models has, of course, to be checked by comparison with sets of numerical simulations (Liljeström et al. 2009). Combining such closures with (dynamically quenched) mean-field dynamo models will ultimately allow to develop a consistent sub-grid scale framework, potentially enabling global large-eddy simulations of ionised accretion discs.

In the following, we aim to demonstrate that there exist helicity-based dynamo mechanisms in stratified MRI simulations which are consistent with the observed rising field structures.

2 NUMERICAL SETUP

We follow the non-linear evolution of ZNF stratified MRI by solving the standard visco-resistive MHD equations,

$$\begin{aligned} \partial_t \rho + \nabla \cdot (\rho \mathbf{v}) &= 0, \\ \partial_t (\rho \mathbf{v}) + \nabla \cdot [\rho \mathbf{v} \mathbf{v} + p^* \mathbf{I} - \mathbf{B} \mathbf{B}] &= 2\rho \Omega (q \Omega x \hat{\mathbf{x}} - \hat{\mathbf{z}} \times \mathbf{v}) - \rho \nabla \Phi(z) \hat{\mathbf{z}} \\ &\quad + \rho \nu \nabla \cdot [\nabla \mathbf{v} + (\nabla \mathbf{v})^\top - 2/3 \nabla \cdot \mathbf{v} \mathbf{I}], \\ \partial_t \mathbf{B} - \nabla \times (\mathbf{v} \times \mathbf{B} - \eta \nabla \times \mathbf{B}) &= 0, \end{aligned}$$

neglecting the effects of self-gravity and radiative transport. Assuming an isothermal equation of state, the stratification is thus fully defined by a static potential $\Phi(z)$. The total pressure $p^* = p + 1/2 \mathbf{B}^2$, all other symbols have their usual meanings. In the following, we will mainly refer to the Lagrangian velocity $\mathbf{u} = \mathbf{v} - q \Omega x \hat{\mathbf{y}}$. We focus on the case with box dimensions of $H \times \pi H \times 6H$ at a reso-

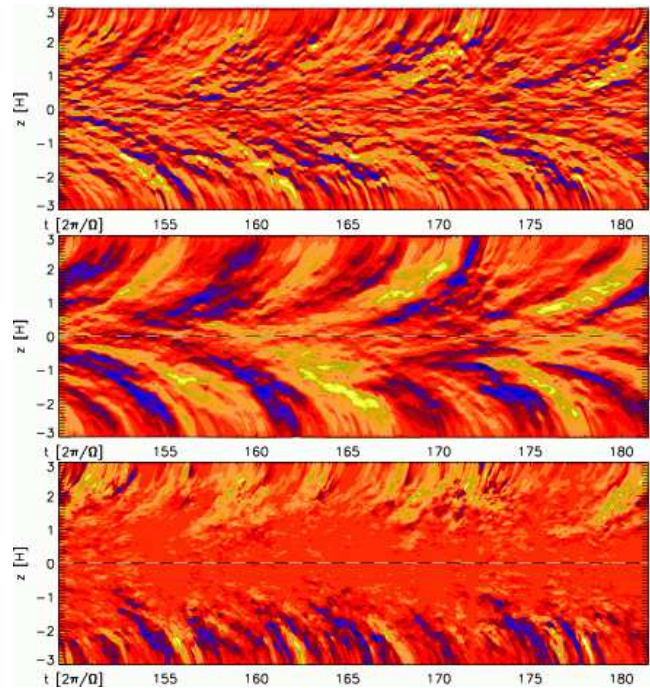


Figure 1. Space time evolution of the horizontally averaged radial field $\bar{B}_r(z, t)$, azimuthal field $\bar{B}_\phi(z, t)$, and magnetic α effect (cf. Sec. 4.1). The colour coding is normalised by the vertical rms amplitude at any given time to remove the stochastic fluctuations in the overall field strength and highlight the coherent pattern.

lution of $96/H$ and chose a fiducial value of $Pm = \nu/\eta = 2$. Applying the spectral analysis described in Sec. 3.1.2 of Fromang et al. (2007), we check that our choice of $Re = H^2 \Omega \nu^{-1} = 6250$ is reasonably resolved, i.e., that the estimated dissipation rate due to the numerical truncation error is lower than the one given by the explicit dissipation.

For our simulations, we use the second order Godunov code NIRVANA (Ziegler 2004) which has been extended and tested for the shearing box formalism (Gressel & Ziegler 2007). Since MRI turbulence is inherently sub-Alfvénic and transonic, accurate treatment of the underlying MHD waves is mandatory. To improve the effective resolution of our code at discontinuities, we implemented the HLLD Riemann solver of Miyoshi & Kusano (2005).

Our vertical boundary conditions (BCs) are of the outflow type. This allows the field to escape the box rather than pile-up and overshoot as in the case of periodic vertical BCs (e.g. Stone et al. 1996; Davis et al. 2009). For reasons of robustness, the radial and azimuthal field components are set to zero at these boundaries, which notably leads to the formation of a disc “wind” as seen in panel (b) of Fig. 5. Zero-gradient BCs in these fields work equally well but no wind is seen in this case (also cf. Suzuki & Inutsuka 2009). Apart from this, the features we are concerned with in this study are, however, largely independent of the boundaries (and the vertical extent of the box) and have been observed with various types of BCs: potential field (Brandenburg 2008), outflow (Miller & Stone 2000), and solving a characteristic equation (Suzuki & Inutsuka 2009).

One argument in favour of periodic boundaries is that they conserve the azimuthal and radial flux and therefore do not “pollute” the dynamo-generated field via an inward Poynting flux $S = \mathbf{E} \times \mathbf{B}$. We have checked that for $S_z = B^2 v_z - \mathbf{B} \cdot \mathbf{v} B_z$, the dominant

contribution is from the advective term, and thus the net Poynting flux is directed outwards. To compensate for the mass loss through the open boundaries and provide a stationary background with respect to the hydrostatic equilibrium, we implemented a continuous mass supply similar to the one suggested by Hanasz et al. (2009).

3 SIMULATION RESULTS

In the middle panel of Figure 1, we plot the temporal evolution of the mean toroidal field $\bar{B}_y(z, t)$, showing characteristic cycles on timescales of roughly ten orbits. Such cycles occur naturally in a stratified environment (Brandenburg et al. 1995; Stone et al. 1996; Miller & Stone 2000; Turner 2004; Suzuki & Inutsuka 2009; Johansen et al. 2009; Davis et al. 2009). Similar cycles have been observed in non-stratified boxes with sufficient vertical extent (Lesur & Ogilvie 2008), but it is currently unclear whether these phenomena are related.

The parity of the field is not well defined and changes chaotically from dipole to quadrupole symmetry, with the former prevailing. The intermittent parity suggests that the underlying mechanism operates in a highly non-linear and probably chaotic regime. The most striking feature in Fig. 1, however, are accelerated "updraughts", reminiscent of the solar butterfly diagram.¹

The evolution of the radial field is shown in the upper panel of Fig. 1, where the same upward motion is visible. Unlike the toroidal field, the structures in the space time diagram are much more filamentary (also cf. Fig. 7 in Davis et al. 2009). One is tempted to identify the cycle from the blue and yellow lines, but this is misleading. When looking at a slice at constant time t , these pronounced streaks partly exhibit a bipolar structure in the vertical direction rather than a cyclic behaviour in time. At a given time, these streaks are somewhat reminiscent of MRI channel modes. In fact, the first ones directly emerge out of the initial linear growth phase. It remains open whether such features survive at realistic magnetic Reynolds numbers, R_m . Ignoring the high contrast features, the same cycle as in B_y becomes visible in red and orange colours.

Currently, there exist two scenarios which try to explain these characteristic field patterns: on the one hand, it has been speculated that the origin of these upward motions is buoyant rise due to Parker-unstable toroidal fields (see e.g. Miller & Stone 2000). Alternatively, Brandenburg et al. (1995) have suggested the presence of an $\alpha\Omega$ type mean-field dynamo, which can produce patterns that travel away from the midplane if the α_{yy} component of the dynamo tensor is negative.

In a recent analysis, Shi et al. (2009) show that, several scale heights H away from the midplane, the undulatory Parker instability is responsible for the upward magnetic motions. Near the midplane, however, they find the flow to be buoyantly stable.

In the subsequent analysis, we will show by means of a simple experiment that the field patterns near the midplane are effected by a turbulent electromotive force (EMF). Only beyond $\sim 1.5H$ does the bulk motion of the fluid become the dominant transport process.

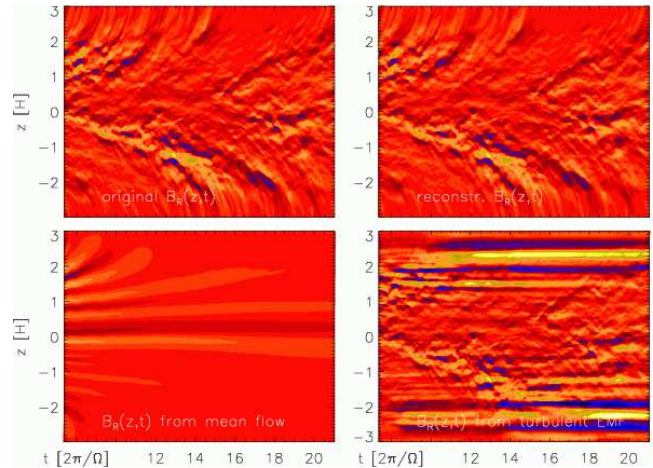


Figure 2. Reconstruction of $\bar{B}_x(z, t)$ from Eq. (1), using space time profiles of $\mathcal{E}(z, t)$ and $\bar{u}_z(z, t)$ stored from the simulation (upper panels, left: original, right: reconstructed). By individually discarding the two induction terms, we investigate the origin of the upward motions (lower panels, left: effect of mean flow, right: effect of turbulent EMF). Near the midplane, the field patterns are evidently due to the EMF. Buoyancy becomes dominant above $z \sim 1.5H$.

3.1 Mean-field description

For a differentially rotating medium, the mean-field induction equation of resistive MHD in the local Hill system reads

$$\partial_t \bar{\mathbf{B}} = \nabla \times \left[\bar{\mathbf{u}} \times \bar{\mathbf{B}} + \overline{\mathbf{u}' \times \mathbf{B}'} + (q\Omega x \hat{\mathbf{y}}) \times \bar{\mathbf{B}} - \eta \nabla \times \bar{\mathbf{B}} \right], \quad (1)$$

with η the molecular diffusivity, and where overbars denote horizontal averages, and primes denote the corresponding fluctuations in the fluid velocity \mathbf{u} , and magnetic field \mathbf{B} . The shear parameter q takes the value of $-3/2$ for the case of a Keplerian rotation profile.

We want to stress that this formulation does not make any closure assumptions, which means Eq. (1) is exact.² The effect of the turbulence on the mean field is expressed by the correlation $\mathcal{E} = \overline{\mathbf{u}' \times \mathbf{B}'}$, i.e., the mean of the cross product of the fluctuating velocity and magnetic field.

In the upper two panels of Fig. 2, we demonstrate that the collapsed profiles $\mathcal{E}_y(z, t)$ and $\bar{u}_z(z, t)$ contain all the information to restore the mean radial field via Eq. (1), more specifically

$$\partial_t \bar{B}_x = \partial_z (\bar{u}_z(z, t) \bar{B}_x) + \mathcal{E}_y(z, t) - \eta \partial_z \bar{B}_x. \quad (2)$$

This implies that (in our 1D approach) only $\partial_z \mathcal{E}_y$ is relevant to sustain \bar{B}_x – note that on the contrary Davis et al. (2009) find indications that $\partial_y \mathcal{E}_z$ may also play a role in replenishing the radial field. This does, however, not seem to have an effect on horizontally averaged quantities.

Since $\partial_t \bar{B}_y$ is dominated by stretching of the radial field via the shear term, we focus on the reconstruction of \bar{B}_x , where only the first two terms in Eq. (2) act as sources. By individually discarding these terms, we examine their effect on the observed field pattern. If the turbulent EMF is omitted (third panel in Fig. 2), the initial field decays. Field advection is only apparent away from the midplane, which is consistent with the results of Shi et al. (2009). If, on the

¹ We caution the reader to bear in mind that this phenomenon might be specific to the local box geometry, which is the scope of this analysis.

² Given the cross terms $\overline{\mathbf{u}' \times \bar{\mathbf{B}}}$ and $\overline{\bar{\mathbf{u}} \times \mathbf{B}'}$ vanish, which is the case if the chosen averages comply with the Reynolds rules (idempotence of the averaging operator, vanishing means of fluctuations) as is trivially fulfilled for arithmetic averages.

other hand, we suppress the mean fluid motion $\bar{\mathbf{u}}$ and only consider $\bar{\mathbf{u}}' \times \mathbf{B}'$ (fourth panel in Fig. 2), we can still accurately reconstruct the rising field structures near the midplane.

Away from the midplane, this approach is, of course, inconsistent, and we would have to advect $\mathcal{E}(z, t)$ with $-\bar{\mathbf{u}}$ to match it with $\bar{\mathbf{B}}$ in a Lagrangian sense. The resulting grooves are again reminiscent of MRI channel modes – which are in fact valid solutions to the 1D mean-field equation. In this respect, the scale separation is blurred as one would naturally attribute such a small-scale effect to the fluctuating field.

4 TOWARDS A POSSIBLE ACCRETION DISC DYNAMO

In the following, we set out to describe the cyclic behaviour in a more generalised way, i.e., without a need for the time-dependent electromotive forces from the direct simulations. To do so, we need to apply a closure model to Eq. (1). This is typically done in the form of constant parameters which express the turbulent EMF in terms of the mean field and its gradients. The introduced abstraction is analogous to the α viscosity for the accretion stresses and subsumes the effects of unresolved scales. Ultimately, the universality of these parameters (or rather, their scaling with respect to the relevant dimensionless numbers) needs to be probed. As a first approach, we here apply a formulation which only retains vertical derivatives (Brandenburg 2005):

$$\mathcal{E}_i = \alpha_{ij} \bar{B}_j - \tilde{\eta}_{ij} \varepsilon_{jkl} \partial_k \bar{B}_l, \quad i, j \in \{x, y\}, k = z. \quad (3)$$

If we substitute this closure into the mean-field induction equation (1), we obtain the standard $\alpha\Omega$ dynamo model, where the diagonal elements of the α tensor give rise to a feedback loop enabling exponential field amplification. In more detail, α_{yy} describes the generation of poloidal field from toroidal field via $\mathcal{E}_y = \alpha_{yy} \bar{B}_y$. Because of the dominant shear term in the azimuthal field equation, α_{xx} is usually sub-dominant for the operation of an $\alpha\Omega$ type dynamo. Note, however, that the generation of azimuthal fields, of vertical wave number k_z , is regulated by a term ($\alpha_{xx} k_z + q\Omega$), such that the radial α effect can provide a saturation mechanism. We remark that this is potentially interesting in view of the shear rate-dependence of the Maxwell-to-Reynolds stress ratio (Pessah et al. 2006b).

Neglecting the second term in Eq. (3), a simple approximation to α_{yy} can be made by measuring the correlation between \bar{B}_y and \mathcal{E}_y . This has now been done by various authors (Brandenburg et al. 1995; Ziegler & Rüdiger 2001; Brandenburg & Sokoloff 2002; Davis et al. 2009), who find a negative (positive) value for α in the top (bottom) half of the box. Brandenburg et al. (1995) remark that this effect has the wrong sign with respect to what would be expected from quasi-linear theory in the case of stratified rotating turbulence (Rüdiger & Kitchatinov 1993, hereafter RK93). This has later been explained in terms of magnetic buoyancy (Brandenburg 1998), and the idea was subsequently confirmed by Rüdiger & Pipin (2000). In the course of the following analysis, we further elucidate this discrepancy by showing that there exist two distinct *indirect* dynamo mechanisms.

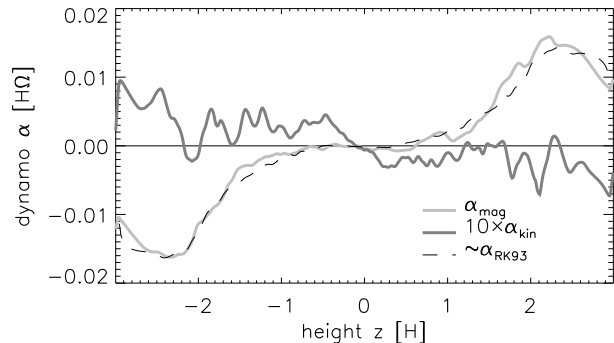


Figure 3. Helical α effect based on the current helicity (light grey) and kinetic helicity (dark grey). Both quantities are highly fluctuating in time but show a systematic average which follows the shape (dashed line) of the effect predicted for stratified, rotating turbulence by RK93.

4.1 Kinetic and magnetic torsality

Quasi-linear theory (Krause & Rädler 1980) states that for isotropic homogeneous turbulence there exists a kinematic α effect

$$\alpha_{\text{kin}} = -\frac{1}{3} \tau_c \overline{\mathbf{u}' \cdot \text{curl}(\mathbf{u}')}. \quad (4)$$

This term is derived from a closure in the induction equation to obtain an approximation for $\partial_t \mathcal{E}^{\text{kin}} = \bar{\mathbf{u}}' \times \partial_t \bar{\mathbf{B}}'$, and describes the leading-order effect of an imposed helical velocity field. As such, the kinematic α neglects any feedback due to the magnetic field itself. Considering the effect of the Lorentz force in the momentum equation, Pouquet, Frisch & Leorat (1976) derive a similar term for $\partial_t \mathcal{E}^{\text{mag}} = -\bar{\mathbf{B}}' \times \partial_t \bar{\mathbf{u}}'$, which leads to an analogous magnetic α effect proportional to the current helicity density $h_{\text{mag}} = \mathbf{B}' \cdot \text{curl}(\mathbf{B}')/\mu_0$ of the small-scale field,

$$\alpha_{\text{mag}} = \frac{1}{3} \tau_c \overline{\mathbf{u}'_A \cdot \text{curl}(\mathbf{u}'_A)}, \quad (5)$$

where $\mathbf{u}'_A = \mathbf{B}' / \sqrt{\mu_0 \varrho}$ is the fluctuation Alfvén velocity. Approaching equipartition field strength, both terms are equally important and add-up to an effective $\alpha = \alpha_{\text{kin}} + \alpha_{\text{mag}}$. It is now a common notion in dynamo theory that α_{kin} takes the role of the driver, while α_{mag} describes a non-linear response, building up gradually and ultimately quenching the kinematically imposed forcing. This process is a consequence of the conservation of magnetic helicity and was termed *dynamical quenching* (Blackman & Brandenburg 2002). However, see Courvoisier et al. (2009) for an alternative method with a more symmetric treatment of the momentum and induction equations. While such an approach might be necessary in the presence of a magnetic instability, we believe that the secondary large-scale dynamo effects are well described by the dynamical quenching formalism.

In Fig. 3, we plot time averaged profiles for the two quantities defined in Eqs. (4) and (5) – also see the lower panel of Fig. 1. Both torsalities are dominated by strong rms fluctuations but show a systematic residuum if averaged over times long compared to the cycle period. The magnetic term dominates and strikingly shows exactly the shape that is expected for stratified rotating turbulence (Rüdiger & Kitchatinov 1993):

$$\alpha_{\text{RK93}} = -\tau_c^2 \Omega \overline{u'^2} (\Psi^\rho \nabla \log \rho + \Psi^\mu \nabla \log u'), \quad (6)$$

with rotational quenching functions $\Psi^\rho(\hat{\Omega})$ and $\Psi^\mu(\hat{\Omega})$, weakly de-

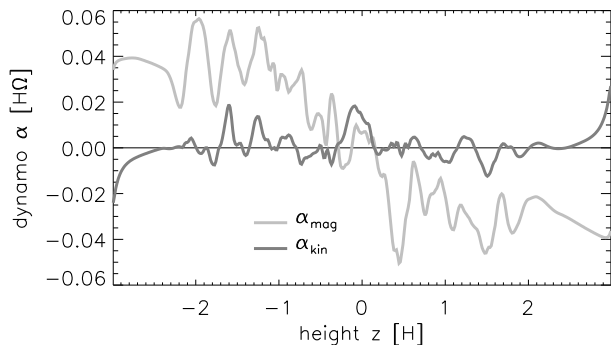


Figure 4. Same as Fig. 3, but for a short time interval during the linear growth phase at the beginning of the simulation. Note the opposite sign of α_{mag} effected from MRI modes.

pending on the Coriolis number $\hat{\Omega} = 2\tau_c\Omega$ of the flow.³ Because of the excellent agreement, we attribute this positive α effect to a Parker-type instability. While we find the sign of α_{mag} to be robust in all our simulations, the sign of α_{kin} curiously shows no preference for the aligned or anti-aligned state.

To fix the free parameter in Eqs. (4) and (5), we roughly estimate τ_c from a fit to the quasi-linear approximation $\eta_t \simeq \tau_c/3 \mathbf{u}'^2$ – cf. panel (c) of Fig. 5 – from which we infer a correlation time $\tau_c \simeq 0.2\Omega^{-1}$, corresponding to $\hat{\Omega} = 0.4$. To explain the observed amplitude in α_{mag} , one however has to assume a coherence time $\tau_c^p \simeq 2.2\Omega^{-1}$ for the effect in Eq. (6), which is enhanced by a factor of ~ 10 compared to the local coherence time. If this effect is caused by a Parker dynamo (Parker 1992) operating above $z \sim 1.5H$, which is consistent with the analysis of Shi et al. (2009), the existence of a longer global turnover time scale should however not be surprising.

Our amplitude of $\alpha_{\text{mag}} \sim 0.02H\Omega$ is comparable to the value measured by Johansen & Levin (2008) for a strongly magnetised accretion disc. Moreover, Johansen & Levin find indications for a *fast* dynamo, i.e., an increased effect for higher Rm. This would imply that current simulations possibly underestimate the saturation level of the turbulence. Finally, our value for τ_c^p is also very similar to the one estimated for zonal flows by Johansen et al. (2009).

The characteristic shape of the α profile in Fig. 3 can be seen as an indication that the effect is not caused by the MRI in an un-intermediate way, but simply via the stratified turbulence it creates. This notion finds further support when looking at the initial linear growth stage of the MRI (see Fig. 4), where we observe a strong α_{mag} with the opposite sign. Moreover, the distinct peaks in the profile can clearly be identified with the MRI channels. Note that the tendency of these features to migrate away from the midplane is consistent with the negative sign of their magnetic torsality. Figures 3 and 4 taken together support the conjecture that there are *direct* and *indirect* dynamo mechanisms operating in stratified MRI turbulence (cf. Blackman & Tan 2004).

4.2 Test field method

In the past years, the so-called test field (TF) method (Schrunner et al. 2005; Brandenburg et al. 2008) has been established as a standard tool to measure turbulent dynamo effects. The

method solves, simultaneously to the actual MHD simulation, a set of ν additional induction equations

$$\partial_t \mathcal{B}'_{(\nu)} = \nabla \times [\mathbf{u}' \times \bar{\mathcal{B}}_{(\nu)} + (\bar{\mathbf{u}} + q\Omega x \hat{\mathbf{y}}) \times \mathcal{B}'_{(\nu)} - \overline{\mathbf{u}' \times \mathcal{B}'_{(\nu)}} + \mathbf{u}' \times \mathcal{B}'_{(\nu)} - \eta \nabla \times \mathcal{B}'_{(\nu)}], \quad (7)$$

for the TF fluctuations $\mathcal{B}'_{(\nu)}$. Imposing $\nu = 4$ suitably varying fields $\bar{\mathcal{B}}_{(\nu)}$, one thus obtains 4×2 linearly independent EMF components, which allows to directly solve for the eight unknown tensor coefficients α_{ij} and $\tilde{\eta}_{ij}$.

In a more graphic way, the tracer fields pick-up the linear response of the prescribed field under the effect of the small-scale velocity field \mathbf{u}' . They do not directly see the actual magnetic field of the simulation. However, since the velocity field \mathbf{u}' is subject to the Lorentz force, the method is well capable to capture a magnetically induced α effect. Following Brandenburg (2005), we use the Fourier modes with $k_z = k_1 \equiv 2\pi/L_z$ which should grasp the essential behaviour for the fields seen in Fig 1. The ideal way of determination would be to apply TFs according to a Fourier series (Brandenburg et al. 2008). Due to the growing number of equations, this sets high demands on the computing power and is currently not feasible given the resolution required to resolve the most unstable MRI modes.

Hubbard et al. (2009) have recently demonstrated that the test field method is applicable beyond the kinematic regime. The authors, however, conclude that care has to be taken in interpreting the results if (what they call) a meso-scale dynamo is present. We conjecture that such an effect might be existent in our simulations in the form of localised MRI modes. Whether such a *direct* dynamo is in fact significant, will have to be checked by further investigations.

Because of the non-linear terms in Eq. (7), the test field method is prone to the exponential amplification of small-scale features (Cattaneo & Hughes 2009). This has first been perceived as a source of noise in the determination of the kinematic dynamo effect. As a solution, Sur et al. (2008) and Gressel (2009) suggest to reset the test field fluctuations in regular time intervals. Such an approach has previously been used for the imposed field method (Ossendrijver et al. 2002). Reset time intervals between 0.5 and 8 orbital periods have been tested, and the results are found to depend weakly on the chosen value (also cf. lower panel of Fig. 6 in Hubbard et al. 2009).

4.3 Tensor coefficients from the TF method

The eight coefficients of the dynamo tensors are plotted as a function of z in Fig. 5. Most notably, the toroidal α effect is found to be identical to α_{mag} in Fig. 3, i.e., positive (above the midplane) and follows the analytical profile for stratified rotating turbulence of RK93. Such profiles have also recently been observed in simulations of buoyant galactic turbulence (Gressel et al. 2008).

The shape of the diffusivity tensor $\tilde{\eta}$ (lower two panels) and the relative strength of its components agree well with previous results of Brandenburg (2008), as do the off-diagonal elements of the α tensor (second panel). We remark that Gressel, Ziegler & Elstner (2008) have found a negative kinematic α in both α_{xx} and α_{yy} for the case of stratified Cartesian shear – implying that MRI turbulence neither resembles rotating, nor sheared turbulence. Moreover, unlike expected for a kinematic dynamo, the radial and azimuthal components have opposite signs. This might be indicative of a dynamo in a quenched state. It therefore seems worthwhile to inves-

³ For fast rotation, turbulence becomes anisotropic along the axis of rotation. This is however a minor effect in disc systems where $\hat{\Omega} < 1$.

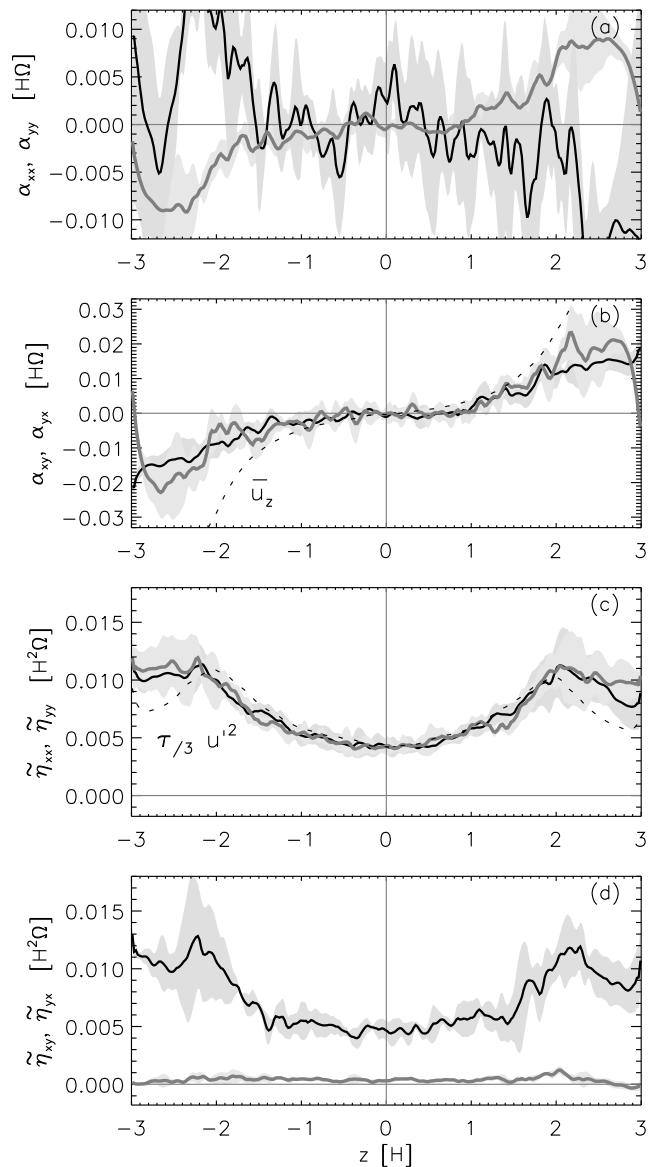


Figure 5. Dynamo coefficients obtained with the TF method. Ordinate labels refer to curves plotted in dark (α_{xx}, \dots) or light (α_{yy}, \dots) colours, respectively. Dashed lines show the mean vertical fluid motion, panel (b), and the quasi-linear estimate for the diffusion profile, panel (c).

tigate whether the ratio of α_{xx} and α_{yy} depends on the shear parameter q in a similar way as does the ratio of Maxwell and Reynolds stresses (Pessah et al. 2006b).

As already mentioned, the azimuthal α effect is positive (negative) in the top (bottom) half of the box for $|z| > H$, but shows the opposite sign near the midplane. This is in agreement with Brandenburg (2008), who found a very similar behaviour. The *negative* α effect near the mid plane can qualitatively be explained by the buoyancy of small-scale flux tubes (Brandenburg 1998).⁴ Even though the effect is comparatively weak, the negative sign near the midplane determines the overall dynamo mode which is required to

⁴ Alternatively, this might simply be the cumulative signature of persistent MRI channel modes (cf. Fig. 4), possibly seen as high-contrast features in the uppermost panel of Fig. 1.

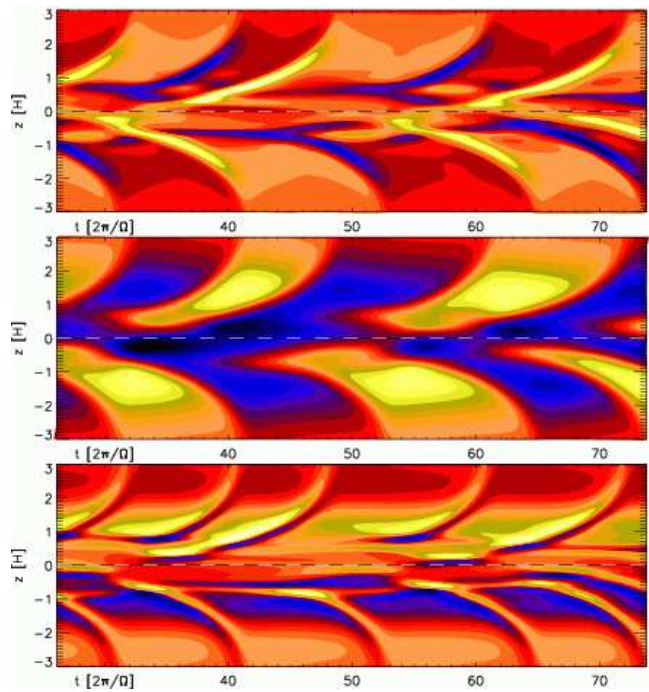


Figure 6. Dynamo patterns from a dynamically quenched 1D mean-field model. Quantities shown are \bar{B}_x (top), \bar{B}_y (middle), and α_{mag} (bottom).

explain the observed direction of propagation (Brandenburg et al. 1995).

Finally, we remark that earlier studies looking at the correlation between \bar{B}_y and \mathcal{E}_y were potentially biased towards regions of strong fields, which is consistent with a negative value for α near the midplane.

4.4 A dynamically quenched dynamo model

If we apply the inferred dynamo profiles to a simple one-dimensional mean-field model, we can successfully reproduce the main features of the butterfly diagram, as is shown in Fig. 6. Note that our approach recovers the asymmetry between the radial and azimuthal field seen in Fig. 1.

Unlike in earlier studies (Brandenburg & Donner 1997; Brandenburg & Sokoloff 2002), and in addition to mean-field equations for $\bar{B}_x(z, t)$ and $\bar{B}_y(z, t)$, we include an equation for $\alpha_{\text{mag}}(z, t)$, the evolution of which is shown in the bottom panel of Fig. 6. The extra equation is motivated by the dynamical quenching formalism, derived by Blackman & Brandenburg (2002) for the case of sheared turbulence. This formalism is founded on the fundamental concept of magnetic helicity conservation. The dynamically evolved value of $\alpha_{\text{mag}}(z, t)$ is, in turn, superimposed to the prescribed kinematic $\alpha_{\text{kin}}(z)$, giving rise to genuinely non-linear behaviour. We hereby closely follow the approach described in Section 2.3 of Brandenburg, Candelaresi & Chatterjee (2009) and implement their Eq. (17) assuming a simple advective helicity flux $\propto \alpha_{\text{mag}}(z, t) \bar{\mathbf{v}}(z)$.

We here want to refrain from describing the related results in detail as the system develops very complex behaviour for high magnetic Reynolds numbers and a careful analysis is due. An extensive study on the transition of the reduced system into chaotic behaviour seems worthwhile.

We point out that the temporal evolution of α_{mag} already bears

some similarity with its counterpart in the direct simulations (cf. Fig. 1), and the overall parity agrees. Moreover, there seems to exist a doubling of the cycle frequency in this quantity, along with a distinct phase pattern with one polarity prevailing. This intermittent pattern is likely related to a phase shift between \bar{B}_x and \bar{B}_y , which is a hallmark of dynamo-generated fields.

The saturated amplitude of $\alpha_{\text{mag}}(z, t)$ is determined by the response to the imposed $\alpha_{\text{kin}}(z)$. This is in agreement with the amplitudes of α_{mag} and α_{xx} in Figs. 3 and 5, respectively. Whether this is the correct direction of causality in real MHD turbulence is as yet not a clear-cut question (see Blackman & Field 2004, for an alternative approach).

5 CONCLUSIONS

As has now been found by a number of authors, vertical stratification can alleviate concerns about non-convergent turbulent stresses in zero net-flux shearing box simulations (see Davis et al. 2009). Along these lines, the idea of large-scale magnetic fields playing an important role in setting the outer scale of the turbulence (Pessah et al. 2007), and hence providing a meaningful amplitude for the viscous stress, has gained new interest. Such fields are the natural outcome of a large-scale dynamo, for which all requirements are met in a stratified shearing box simulation. We propose that the saturation level of turbulent stresses in such a scenario is intimately linked to the saturation of these large-scale fields, making it mandatory to study the related accretion disc dynamo.

In this paper, we have performed local simulations of stratified MRI with zero vertical net-flux. Looking into the kinetic and current helicities and probing the kinematic dynamo via the TF method, we have identified a possible dynamo mechanism to explain the propagation of mean magnetic fields away from the mid plane. Such an alternative explanation is necessary because the flow is found to be stable to Parker instability near the mid plane (Shi et al. 2009), and the pattern speed is independent of the bulk motion of the flow – a finding which strongly supports the interpretation in terms of a dynamo wave.

Moreover, our analysis has brought forward a rather curious idea, namely that there exist (at least) two distinct dynamo mechanisms – one the immediate signature of MRI modes, and one the indirect effect of the resulting turbulence in the presence of stratification. Such a co-existence of a direct and indirect dynamo has already been discussed by Blackman & Tan (2004).

For the *indirect* dynamo, there are two candidates: (i) a classical Parker-type dynamo, i.e., “cyclonic” turbulence effected by the Coriolis force (Rüdiger & Kitchatinov 1993), and (ii) a “buoyant” dynamo caused by the Lorentz force. Such an effect has first been predicted by Brandenburg (1998) and was derived formally by Rüdiger & Pipin (2000). While the former effect (with positive α_{kin}) is presumably dominant in the Parker-unstable halo, the latter (with negative α_{kin}) is likely to operate close to the disc midplane.

Moreover, there is a remarkable resemblance to recent results by Johansen & Levin (2008), who found a similar interplay between the Parker instability and MRI for magnetically dominated accretion discs. Our results similarly suggest to take up the ideas of a self-regulatory dynamo cycle as proposed by Tout & Pringle (1992) almost two decades ago.

Whether this scenario is real, has to be checked by future stud-

ies. We conjecture that the *direct* dynamo should equally be seen in non-stratified simulations as studied by Lesur & Ogilvie (2008).⁵

The central result of our analysis is the relevance of the current helicity as a key indicator for magnetically induced dynamo action (cf. Sec. 3 of Blackman 2010). The picture is far from being conclusive but the results are promising. Contrary to the general scepticism towards kinematic dynamo theory in the context of magnetic instabilities, the extension of mean-field theory with a dynamical saturation mechanism (as demonstrated in Sec. 4.4 by means of a simple 1D dynamo model) could well provide a framework for understanding fully non-linear accretion disc dynamos.

ACKNOWLEDGEMENTS

The author thanks Sebastien Fromang for discussions on improving the numerical scheme and providing his spectral analysis tools. Richard Nelson, Detlef Elstner and Axel Brandenburg are acknowledged for helpful remarks on a draft version of this paper. I also thank the anonymous referee for a careful report that helped to improve the presentation of the paper. This work used the NIRVANA code version 3.3 developed by Udo Ziegler at the Astrophysical Institute Potsdam. All computations were performed on the QMUL HPC facility, purchased under the SRIF initiative.

REFERENCES

- Balbus S. A., Hawley J. F., 1998, *RvMP*, 70, 1
- Blackman E. G., 2010, *Astronomische Nachrichten*, 331, 101
- Blackman E. G., Brandenburg A., 2002, *ApJ*, 579, 359
- Blackman E. G., Field G. B., 2004, *Physics of Plasmas*, 11, 3264
- Brandenburg E. G., Tan J. C., 2004, *Ap&SS*, 292, 395
- Brandenburg A., 1998, in M. A. Abramowicz, G. Bjornsson, & J. E. Pringle ed., *Theory of Black Hole Accretion Disks Disc turbulence and viscosity*. pp 61–+
- Brandenburg A., 2005, *AN*, 326, 787
- Brandenburg A., 2008, *AN*, 329, 725
- Brandenburg A., 2009, *ApJ*, 697, 1206
- Brandenburg A., Candelaresi S., Chatterjee P., 2009, *MNRAS*, 398, 1414
- Brandenburg A., Donner K. J., 1997, *MNRAS*, 288, L29
- Brandenburg A., Nordlund A., Stein R. F., Torkelsson U., 1995, *ApJ*, 446, 741
- Brandenburg A., Rädler K.-H., Schrunner M., 2008, *A&A*, 482, 739
- Brandenburg A., Sokoloff D., 2002, *GApFD*, 96, 319
- Cattaneo F., Hughes D. W., 2009, *MNRAS*, 395, L48
- Courvoisier A., Hughes D. W., Proctor M. R. E., 2009, *astro-ph* 0909.0721
- Davis S. W., Stone J. M., Pessah M. E., 2009, *astro-ph* 0909.1570
- Fromang S., Papaloizou J., 2007, *A&A*, 476, 1113
- Fromang S., Papaloizou J., Lesur G., Heinemann T., 2007, *A&A*, 476, 1123
- Goodman J., Xu G., 1994, *ApJ*, 432, 213
- Gressel O., 2009, PhD thesis, University of Potsdam, (2009)
- Gressel O., Ziegler U., 2007, *CoPhC*, 176, 652
- Gressel O., Ziegler U., Elstner D., 2008, *astro-ph:0811.0542*

⁵ Note, however, that even in the absence of stratification, a dominant bipolar toroidal field might still lead to a sufficient inhomogeneity in the turbulence to provide a gradient in \mathbf{u}' .

- Gressel O., Ziegler U., Elstner D., Rüdiger G., 2008, AN, 329, 619
- Hanasz M., Otmianowska-Mazur K., Kowal G., Lesch H., 2009, A&A, 498, 335
- Hubbard A., Blackman E. G., 2008, MNRAS, 390, 331
- Hubbard A., Del Sordo F., Käpylä P. J., Brandenburg A., 2009, MNRAS, pp 1219–+
- Johansen A., Levin Y., 2008, A&A, 490, 501
- Johansen A., Youdin A., Klahr H., 2009, ApJ, 697, 1269
- King A. R., Pringle J. E., Livio M., 2007, MNRAS, 376, 1740
- Kitchatinov L. L., Rüdiger G., 2009, ArXiv e-prints
- Krause F., Rädler K. H., 1980, Mean-field magnetohydrodynamics and dynamo theory. Oxford: Pergamon Press, 1980
- Latter H. N., Lesaffre P., Balbus S. A., 2009, MNRAS, 394, 715
- Lesur G., Longaretti P.-Y., 2007, MNRAS, 378, 1471
- Lesur G., Ogilvie G. I., 2008, A&A, 488, 451
- Liljeström A. J., Korpi M. J., Käpylä P. J., Brandenburg A., Lyra W., 2009, Astronomische Nachrichten, 330, 92
- Miller K. A., Stone J. M., 2000, ApJ, 534, 398
- Miyoshi T., Kusano K., 2005, JCoPh, 208, 315
- Ogilvie G. I., 2003, MNRAS, 340, 969
- Ossendrijver M., Stix M., Brandenburg A., Rüdiger G., 2002, A&A, 394, 735
- Parker E. N., 1992, ApJ, 401, 137
- Pessah M. E., Chan C., Psaltis D., 2006a, PhRevL, 97, 221103
- Pessah M. E., Chan C., Psaltis D., 2006b, MNRAS, 372, 183
- Pessah M. E., Chan C., Psaltis D., 2007, ApJ, 668, L51
- Pessah M. E., Goodman J., 2009, ApJ, 698, L72
- Pouquet A., Frisch U., Leorat J., 1976, JFM, 77, 321
- Rüdiger G., Kitchatinov L. L., 1993, A&A, 269, 581
- Rüdiger G., Pipin V. V., 2000, A&A, 362, 756
- Schekochihin A. A., Haugen N. E. L., Brandenburg A., Cowley S. C., Maron J. L., McWilliams J. C., 2005, ApJ, 625, L115
- Schrinner M., Rädler K.-H., Schmitt D., Rheinhardt M., Christensen U., 2005, AN, 326, 245
- Shi J.-M., Krolik J. H., Hirose S., 2009, astro-ph 0909.2003
- Stone J. M., Hawley J. F., Gammie C. F., Balbus S. A., 1996, ApJ, 463, 656
- Sur S., Brandenburg A., Subramanian K., 2008, MNRAS, 385, L15
- Suzuki T. K., Inutsuka S.-i., 2009, ApJ, 691, L49
- Tout C. A., Pringle J. E., 1992, MNRAS, 259, 604
- Turner N. J., 2004, ApJ, 605, L45
- Vishniac E. T., 2009, ApJ, 696, 1021
- Ziegler U., 2004, JCoPh, 196, 393
- Ziegler U., Rüdiger G., 2001, A&A, 378, 668